Lattice Boltzmann model of shallow water flows in curved and meandering channels

Article *in* International Journal of Computational Fluid Dynamics · March 2009

DOI: 10.1080/10618560902754924

CITATIONS
25

READS
282

3 authors:

Haifei Liu
Beijing Normal University
41 PUBLICATIONS **276** CITATIONS
SEE PROFILE

J. G. Zhou
Manchester Metropolitan University
90 PUBLICATIONS **2,094** CITATIONS
SEE PROFILE

Ruain Burrows
Cork Institute of Technology
125 PUBLICATIONS **2,372** CITATIONS
SEE PROFILE

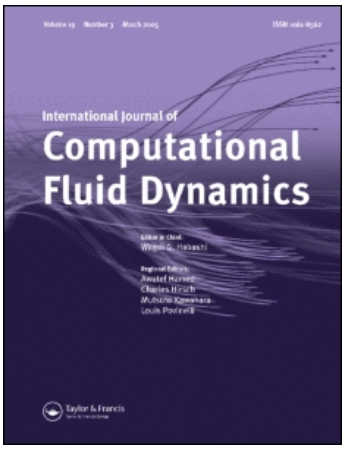

International Journal of Computational Fluid Dynamics
Publication details, including instructions for authors and subscription information:
http://www.informaworld.com/smpp/title~content=t713455064

Lattice Boltzmann model for shallow water flows in curved and meandering channels

Haifei Liu [a]; Guo Jian Zhou [a]; Richard Burrows [a]
[a] Department of Engineering, University of Liverpool, Brownlow Hill, UK

Online Publication Date: 01 March 2009

To cite this Article Liu, Haifei, Zhou, Guo Jian and Burrows, Richard(2009)'Lattice Boltzmann model for shallow water flows in curved and meandering channels',International Journal of Computational Fluid Dynamics,23:3,209 — 220
To link to this Article: DOI: 10.1080/10618560902754924
URL: http://dx.doi.org/10.1080/10618560902754924

International Journal of Computational Fluid Dynamics
Vol. 23, No. 3, March 2009, 209–220

Taylor & Francis
Taylor & Francis Group

Lattice Boltzmann model for shallow water flows in curved and meandering channels

Haifei Liu*, Guo Jian Zhou and Richard Burrows

Department of Engineering, University of Liverpool, Brownlow Hill, L69 3GQ, UK

(*Received 26 September 2008; final version received 10 December 2008*)

Meandering channel flows are simulated using two-dimensional lattice Boltzmann models (LBM) for the shallow water equations. A boundary approach is designed for curved boundary treatment, which is applicable to no-slip, semi-slip and slip boundaries at a second-order accuracy. The large eddy simulation model is added in the lattice Boltzmann model, so that the turbulence can be taken into account and modelled efficiently. The model is verified by three numerical tests: the first two involve flows in meandering channels with 60° and 90° consecutive bends; the third is a 180° sharply curved channel. The numerical results are compared with available experimental data, showing good agreement. This provides a second-order accurate scheme for the LBM to simulate complex flows with curved boundaries.

Keywords: lattice Boltzmann method; large eddy simulation; shallow water flows; meandering channel flow

1. Introduction

Most natural flows are turbulent and three dimensional. In many cases, it is difficult to solve the flow equations with complex flow boundaries. For free surface flows, when the width of the flow is large compared to the depth, the vertical acceleration of water is negligible compared to the gravitational acceleration; hence, the pressure profile with depth is assumed to be hydrostatic. The flow can be described by the shallow water equations, which can be obtained by depth-integration of the Reynolds-averaged Navier-Stokes equations, giving two-dimensional depth-averaged features. The equations are suitable for many practical problems without sharp gradient of water surface or strong secondary flows. Sub-critical flows in meandering open channel are one of the complex flows which can be mathematically modelled using the shallow water equations (Callander 1978). Such flow is common in natural rivers. The flow problem in channel bends is first described by Rozovskii (1961) and later investigated by Yen and Yen (1971). In recent decades, with the development of computing power, numerical models have become popular in both academia and engineering. Morvan *et al*. (2002) simulated meandering compound channel flows using conventional finite volume models. Zarrati *et al*. (2005) developed a mathematical model based on a non-orthogonal curvilinear system and solved it numerically using a finite volume scheme. Additionally, some experiments on meandering channel flows have been carried out, providing valuable measured data (Tamai *et al*. 1983, Tarekul Islam 2000, Tarekul Islam *et al*. 2000) for calibration of a numerical model.

The lattice Boltzmann method is a powerful computational fluid dynamics technique for solving complex fluid flow problems. Based on kinetic theory, the lattice Boltzmann method is first developed by McNamara and Zanetti (1988) to eliminate the numerical noise of the lattice gas automata (LGA) proposed by Frisch *et al*. (1986) for solving the Navier-Stokes equations. Unlike traditional numerical schemes, the lattice Boltzmann method does not discretise the governing equations in space and time, but solves the dynamics of the particles instead. The macroscopic variables are obtained by summing the moments of the distribution functions. A detailed review of the theory and applications of the lattice Boltzmann method have been presented by Chen and Doolen (1998) and Wolf-Gladrow (2000). Incorporating the single relaxation time approximation of the BGK (Bhatnagar, Gross and Krook) model (Bhatnagar *et al*. 1954), Qian *et al*. (1992) and Chen *et al*. (1992) proposed a lattice Boltzmann model (LBM), that has been used in a variety of fields, such as shallow water flows (Zhou 2004), wave modelling (Yan 2000), flow in porous media (Martys and Chen 1996), advection and dispersion (Zhang *et al*. 2002).

*Corresponding author. Email: haifei.liu@liv.ac.uk

ISSN 1061-8562 print/ISSN 1029-0257 online

DOI: 10.1080/10618560902754924
http://www.informaworld.com

With respect to boundary conditions, besides the simple bounce back scheme of first-order accuracy, a number of high-order schemes have been designed for complex geometry (e.g. curved boundary) to improve numerical accuracy and stability. Filippova and Hänel (1998) presented an approach for curved walls, which was later improved by Mei *et al*. (1999). Guo and Zheng proposed an alternative treatment by decomposing the distribution at a curved wall node into equilibrium and the non-equilibrium parts, which is an extension of the extrapolation scheme by Chen *et al*. (1996). Recently, Szalmás (2007) presented a slip boundary treatment to obtain the tangential velocity component for a curved wall. However, these high-order boundary conditions are inconvenient for switching from no-slip to slip boundaries, and inadequate to model semi-slip boundaries.

Therefore, the present study aims to develop a flexible approach applicable to no-slip, semi-slip and slip boundaries for lattice Boltzmann methods, which is then used to simulate meandering channel flows. Providing the depth-averaged features, the non-linear shallow water equations with the large eddy model embedded are selected as the governing equations. The model is verified by three cases illustrated in Figure 1: the first one is a 180° sharply curved channel; the other two concern meandering channels with 60° and 90° consecutive bends, respectively; available experimental data are used to validate the scheme.

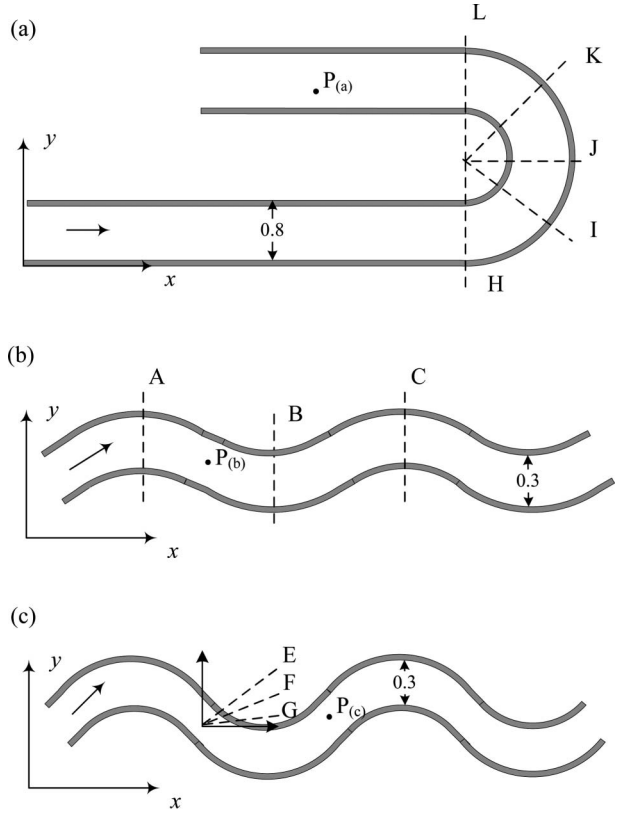

Figure 1. Layout of channels and test sections.

2. Hydrodynamic model

The shallow water equations are widely used to describe the horizontal flows. To provide the detailed structure of the turbulence, large eddy simulation, using space-filtered governing equations with a sub-gird-scale stress model for the unresolved scale stress, is applied for turbulence modelling and can efficiently simulate vorticity larger than a prescribed scale, with only moderate computational effort (Tutar and Hold 2001), so this is used in here.

The general two-dimensional governing equations for shallow water flows can be derived from the Navier-Stokes equations, written in a tensor form as (e.g. Zhou 2004):

$$\frac{\partial h}{\partial t}+\frac{\partial (hu_j)}{\partial x_j}=0 \tag{1}$$

$$\frac{\partial (hu_i)}{\partial t}+\frac{\partial (hu_iu_j)}{\partial x_j}=-\frac{g}{2}\frac{\partial h^2}{\partial x_i}+v_t\frac{\partial^2 (hu_i)}{\partial x_j\partial x_j}+F_i \tag{2}$$

where the Cartesian coordinate system (see Figure 1) and the Einstein summation convention over Latin indices are used; h is water depth; x_j and u_j are the distance and instantaneous space-filtered velocity components in the j direction respectively, i.e. for $j=1$, $x_j=x$ and $u_j=u$; for $j=2$, $x_j=$ y and $u_j=v$. The coordinate directions x and y are oriented along longitudinal and local transverse axes with respect to the channel; and u_j is defined by

$$u_j(x,y,z,t)=\int_{\Delta V} u_j^b G(x,y,z,x',y',z')dV \tag{3}$$

with a spatial filter function

$$G(x,y,z,x',y',z')=\begin{cases}1/\Delta V, & (x',y',z')\in \Delta V\\ 0, & \text{otherwise}\end{cases} \tag{4}$$

and u_j^{b} is the velocity component before space-filtered; $\Delta V=\Delta x'\Delta y'\Delta z'$; x', y' and z' are the coordinates of the space chosen for the velocity filter; $g=9.81\ \mathrm{m/s^2}$ is gravitational acceleration; t is time; v_{t} is the total viscosity ($=v_{\mathrm{k}}+v_{\mathrm{e}}$); v_{k} is the kinematic viscosity; v_{e} is the eddy viscosity, defined by

$$v_{\mathrm{e}}=(C_{\mathrm{s}}l_{\mathrm{s}})^2\sqrt{S_{ij}S_{ij}} \tag{5}$$

where C_{s} is the Smagorinsky constant, l_{s} is the characteristic length scale ($C_{\mathrm{s}}=0.3$ and $l_{\mathrm{s}}=\Delta x$ in

the present study) and S_{ij} is the magnitude of the large scale strain-rate tensor,

$$S_{ij} = \frac{1}{2h}\left[\frac{\partial(hu_i)}{\partial x_j} + \frac{\partial(hu_j)}{\partial x_i}\right] \tag{6}$$

The depth-averaged subgrid-scale stress τ_{ij} with eddy viscosity is calculated by

$$\tau_{ij} = 2v_e h S_{ij} \tag{7}$$

In addition, F_i is the force term defined as:

$$F_i = -\frac{\tau_{bi}}{\rho} - gh\frac{\partial z_b}{\partial x_i} \tag{8}$$

where z_b is bed elevation above datum. The bed shear stress τ_{bi} in the i direction is given by the depth-averaged velocities,

$$\tau_{bi} = \rho C_b u_i \sqrt{u_j u_j} \tag{9}$$

in which C_b is the bed friction coefficient.

3. Lattice Boltzmann model

A lattice Boltzmann model has three main components: the kinetic equation; a lattice pattern and the equilibrium distributions. The lattice Boltzmann model for non-linear shallow water equations with turbulence (LABSWE^{TM}) has been presented by Zhou (2002). After incorporating the subgrid-scale model, for the i direction the lattice Boltzmann equation with a 9-speed square lattice and force term is

$$f_\alpha(x_i + e_{\alpha i}\Delta t, t + \Delta t) = f_\alpha(x_i, t) - \frac{1}{\tau_t}[f_\alpha(x_i, t) - f_\alpha^{eq}(x_i, t)] + \frac{\Delta t}{6e^2} e_{\alpha i} F_i \tag{10}$$

where f_α is the particle distribution function; $e = \Delta x/\Delta t$; Δx is the lattice size; Δt is the time step; $\tau_t = \tau + \tau_e$ is the total relaxation time, wherein τ is the single relaxation time and τ_e is the eddy relaxation time with respect to the eddy viscosity which can be calculated as

$$\tau_e = \frac{-\tau + \sqrt{\tau^2 + 18C_s^2/(e^2 h)\sqrt{\prod_{ij}\prod_{ij}}}}{2} \tag{11}$$

The viscosity of the fluid is calculated by

$$v_t = \frac{\Delta x e}{6}(2\tau_t - 1) \tag{12}$$

In Equation (11),

$$\prod_{ij} = \sum_\alpha e_{\alpha i} e_{\alpha j}(f_\alpha - f_\alpha^{eq}); \tag{13}$$

$e_{\alpha i}$ is the i directional component of the velocity vector of a particle in the α link. For the 9-speed square lattice shown in Figure 2, each particle moves one lattice unit at its velocity along one of the eight links indicated with number 1–8, or else 0 indicates the particle at rest with zero speed. The velocity vector of particles is defined by

$$e_\alpha = \begin{cases} (0,0), & \alpha = 0 \\ e\left[\cos\frac{(\alpha-1)\pi}{4}, \sin\frac{(\alpha-1)\pi}{4}\right], & \alpha = 1,3,5,7 \\ \sqrt{2}e\left[\cos\frac{(\alpha-1)\pi}{4}, \sin\frac{(\alpha-1)\pi}{4}\right], & \alpha = 2,4,6,8 \end{cases} \tag{14}$$

The local equilibrium distribution function is expressed as

$$f_\alpha^{eq} = \begin{cases} W_\alpha\left[\frac{9}{4} - \frac{15gh}{8e^2} - \frac{3}{2e^2}u_i u_i\right]h, & \alpha = 0 \\ W_\alpha\left[\frac{3gh}{2e^2} + \frac{3}{e^2}e_{\alpha i}u_i + \frac{9}{2e^4}e_{\alpha i}e_{\alpha j}u_i u_j - \frac{3}{2e^2}u_i u_i\right]h, & \text{otherwise} \end{cases} \tag{15}$$

where

$$W_\alpha = \begin{cases} \frac{4}{9}, & \alpha = 0 \\ \frac{1}{9}, & \alpha = 1,3,5,7 \\ \frac{1}{36}, & \alpha = 2,4,6,8 \end{cases} \tag{16}$$

From the distribution function, the water depth h and flow velocity u_i can be calculated from

$$h = \sum_\alpha f_\alpha, \quad u_i = \frac{1}{h}\sum_\alpha e_{\alpha i} f_\alpha. \tag{17}$$

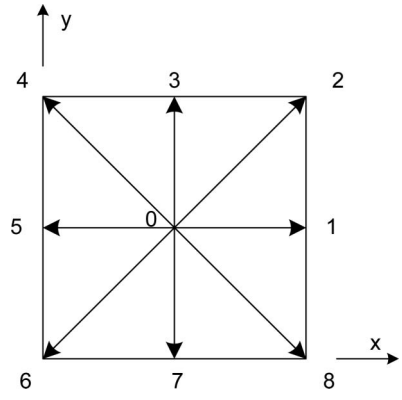

Figure 2. Lattice pattern D2Q9.

4. Boundary conditions

The discrete particle distribution must satisfy imposed constraints for water depth and momentum along the boundaries of the lattice. Over the last 15 years, much research on boundary conditions has been carried out (Ziegler 1993, Maier *et al.* 1996), demonstrating that boundary conditions may influence the accuracy of simulation, and even the numerical stability (Succi 2001). In this section, a flexible scheme for curved boundary conditions is described. It is based on a second-order bounce back and reflection scheme and can be applied to semi-slip and slip boundaries as well.

4.1. No-slip boundary condition

A curved boundary, lying between the fluid nodes (subscript '*f*') and the wall node (subscript '*w*') within the uniform lattice denoted by '○' and '●' respectively, is sketched in Figure 3. Following Filippova and Hänel's philosophy (1998), if the boundary wall is static, the distribution function bouncing back from wall node (N_w) to the fluid node (N_f) may be presented as,

$$\tilde{f}_\alpha(x_f, t+\Delta t) = [(1-\lambda)f_\alpha(x_f,t) + \lambda\, f_\alpha^{eq}(x_f,t)](1-\chi_\alpha) + a_1\chi_\alpha\, f_\alpha^{eq}(x_w,t) + a_2\chi_\alpha\, f_\alpha^{eq}(x_f,t) \tag{18}$$

where λ is the relaxation parameter in N_f, $a_1^2 + a_2^2 = 1$ and $a_1 \cdot a_2 = 0$. The link between nodes N_f and N_w intersects the physical wall boundary at node N_b . If a fraction is defined as

$$\phi = \left|\frac{x_f - x_b}{x_f - x_w}\right|, \tag{19}$$

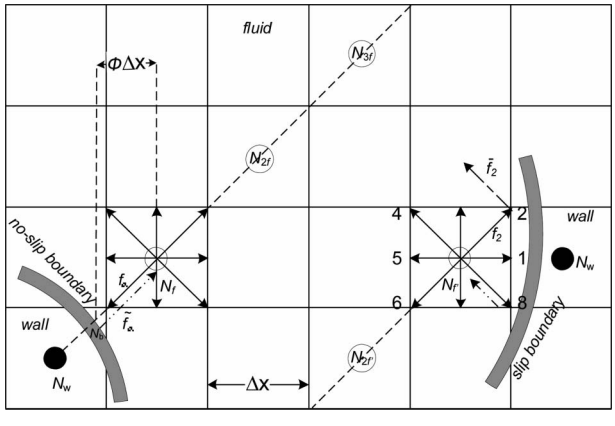

Figure 3. Curved boundary and lattice nodes for no-slip and slip boundaries.

the adjusting parameter χ_α can be calculated by

$$\chi_\alpha = \begin{cases} \lambda(2\phi-1), a_1 = 1, a_2 = 0; & \text{for } \phi \geq 0.5 \\ \lambda\,\frac{2\phi-1}{1-\lambda}, a_1 = 0, a_2 = 1; & \text{for } \phi < 0.5 \end{cases} \tag{20}$$

The equilibrium functions at node N_w,$f_\alpha^{eq}(x_w,t)$, are reasonably assumed to have similar expressions to node N_f (i.e. Equation 15), provided that the u_w, v_w and h_w are obtained by extrapolation from corresponding values of the inside fluid nodes. The macroscopic velocity components at the wall boundary can be estimated using linear extrapolation, as follows.

$$u_w^{(1)} = \frac{(\phi-1)u_f}{\phi}, \quad \text{or} \quad u_w^{(2)} = \frac{(\phi-1)u_{2f}}{1+\phi} \tag{21}$$

Generally, it is more accurate to use $u_w^{(1)}$ than $u_w^{(2)}$ to estimate u_w . However, when ϕ is small, the absolute value of $u_w^{(1)}$ will be very large and lead to numerical instability in the computation, as suggested by Guo *et al.* (2002). To be consistent with the definition of χ_α, a good estimation of velocities can be obtained by

$$u_w = \begin{cases} u_w^{(1)}, & \phi \geq 0.5 \\ \phi u_w^{(1)} + (1-\phi)u_w^{(2)}, & \phi < 0.5 \end{cases} \tag{22}$$

Since the water depth, h, at the boundary is not explicit, a three-point Lagrangian formula is applied in the water depth extrapolation (Mechlih and Hay 1994).

$$h_w = \sum_{p=1}^{3}\left[h(x_p)\prod_{q=1,q\neq p}^{3}\frac{x_w - x_q}{x_p - x_q}\right] \tag{23}$$

If h is extrapolated for the value at x_w (see Figure 4), Equation (23) may be expressed as

$$h_w = h_{3f}\frac{(x_w - x_{2f})(x_w - x_f)}{(x_{3f} - x_{2f})(x_{3f} - x_f)} + h_{2f}\frac{(x_w - x_{3f})(x_w - x_f)}{(x_{2f} - x_{3f})(x_{2f} - x_f)} + h_f\frac{(x_w - x_{3f})(x_w - x_{2f})}{(x_f - x_{3f})(x_f - x_{2f})} \tag{24}$$

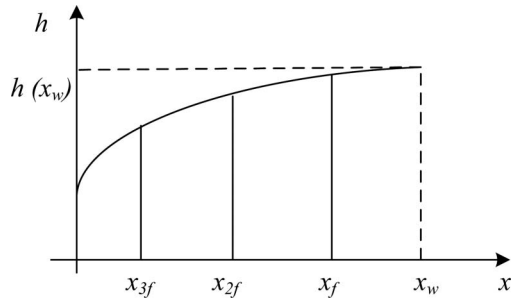

Figure 4. Sketch for three-point Lagrangian extrapolation.

Since x_f, x_{2f} and x_{3f} can be expressed in terms of x_w and Δx

$$\begin{cases} x_f = x_w - \Delta x \\ x_{2f} = x_w - 2\Delta x \\ x_{3f} = x_w - 3\Delta x \end{cases} \tag{25}$$

the following equation can be obtained after the substitution of Equation (25) into Equation (24) and will be used for temporal interpolations.

$$h_w = h_{3f} - 3h_{2f} + 3h_f \tag{26}$$

4.2. Semi-slip and slip boundary conditions

Physically, there is a large flow gradient in the vicinity of a solid boundary for turbulent flows due to wall friction. It cannot be correctly modelled with no-slip boundary conditions, and it is better to use semi-slip boundary conditions in the mathematical model. The wall shear stress, τ_w, may be represented by (Zhou and Goodwill 1997)

$$\tau_{wi} = -\rho C_w u_i \sqrt{u_j u_j} \tag{27}$$

where C_w is the friction factor at the wall. The force term F_i is changed correspondingly,

$$F_i = -\frac{\tau_{bi}}{\rho} - gh\frac{\partial z_b}{\partial x_i} + \frac{\tau_{wi}}{\rho} \tag{28}$$

With respect to the distribution function in the lattice Boltzmann model, the idea of the combination of bounce-back and specular reflection is adopted. A reflection ratio, ξ_i, describes the amount of particles reflected, where i is equal to the index of the total bounced-back distribution function (i.e. $i = 5$ for the current case in Figure 3).

$$\begin{cases} f_4 = \xi_5 \bar{f}_2 + (1-\xi_5)\tilde{f}_8 \\ f_6 = \xi_5 \bar{f}_8 + (1-\xi_5)\tilde{f}_2 \\ f_5 = \tilde{f}_1 \end{cases} \tag{29}$$

where $\bar{f}_\alpha$ represents the purely reflected f_α, which can be estimated to second order accuracy (Bouzidi *et al.* 2001). Taking $\bar{f}_2$ for example, it is (see Figure 3):

$$\bar{f}_2(x_{f'}, t+\Delta t) = \begin{cases} \frac{1}{2\phi} f_2(x_{f'}, t) + \frac{2\phi-1}{2\phi} f_4(x_{f'}, t), & \phi \geq 0.5 \\ 2\phi f_2(x_{f'}, t) + (1-2\phi) f_2(x_{2f'}, t), & \phi < 0.5 \end{cases} \tag{30}$$

The other unknown reflected distribution functions can also be obtained in a similar way. Then, the condition for the distribution functions is formulated in the equation of the tangential momentum balance.

$$f_4 e_{4y} + f_6 e_{6y} = \xi_5 \bar{f}_2 e_{4y} + (1-\xi_5)\tilde{f}_8 e_{4y} + \xi_5 \bar{f}_8 e_{6y} + (1-\xi_5)\tilde{f}_2 e_{6y} = 0 \tag{31}$$

Therefore,

$$\xi_5 = \frac{\tilde{f}_2 - \tilde{f}_8}{(\bar{f}_2 - \bar{f}_8) - (\tilde{f}_2 - \tilde{f}_8)} \tag{32}$$

This approach is repeatedly used to update the corresponding distribution functions along the boundaries. It should be noted that if ξ is set as 1, only the distribution function reflected by the boundary forms, the unknown distribution function and the scheme works as a slip boundary condition. On the contrary, if ξ is equal to zero, it is the bounce-back scheme for a no-slip boundary, as presented in Section 4.1.

4.3. Stability conditions

As a discrete form of a numerical method, the LABSWE may suffer from a numerical instability (Sterling 1996). Based on the discussion by Zhou (2004), some basic conditions should be satisfied to keep numerical stability:

(1) the single relaxation time should be larger than 0.5 ($\tau > 0.5$);
(2) the resultant velocity is smaller than the speed of sound ($u_j u_j < e^2$);
(3) the wave speed in shallow water is smaller than the speed of sound ($gh < e^2$);
(4) the resultant velocity is smaller than the wave speed (i.e. the Froude number Fr < 1).

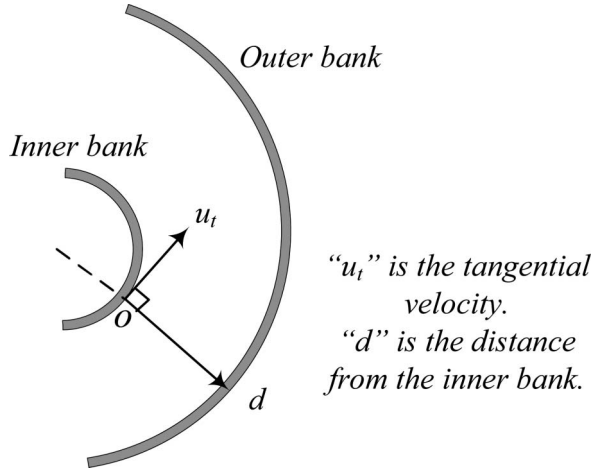

Figure 5. Coordinates layout for a curved channel section.

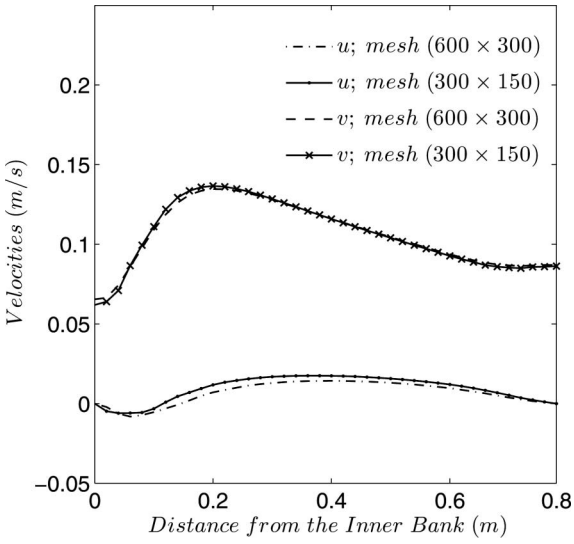

Figure 6. Comparison of the depth-averaged velocities across Section J (Figure 1) of the 180° sharply curved channel.

5. Numerical tests

The two-dimensional numerical model with different boundary conditions described above is now to be validated for three numerical tests: the first one is a 180° sharply curved channel; the other two are meandering channels having 60° and 90° consecutive bends, respectively (see Fig. 1). The coordinates of a channel section at a bend are sketched in Figure 5.

5.1. *Test 1: 180° sharply curved channel*

This case concerning flow in a sharply curved channel represents one of the most complex flows encountered in a natural meandering river. In this test, the flow in a 180° sharply curved channel has been investigated, which is the same as Run No. 8 of Rozovskii's (1961) experiments. The channel is 0.8 m wide and has a 0.4 m internal radius. The bed slope is zero. The entrance water depth is 0.063 m for 0.0123 m^3/s flow

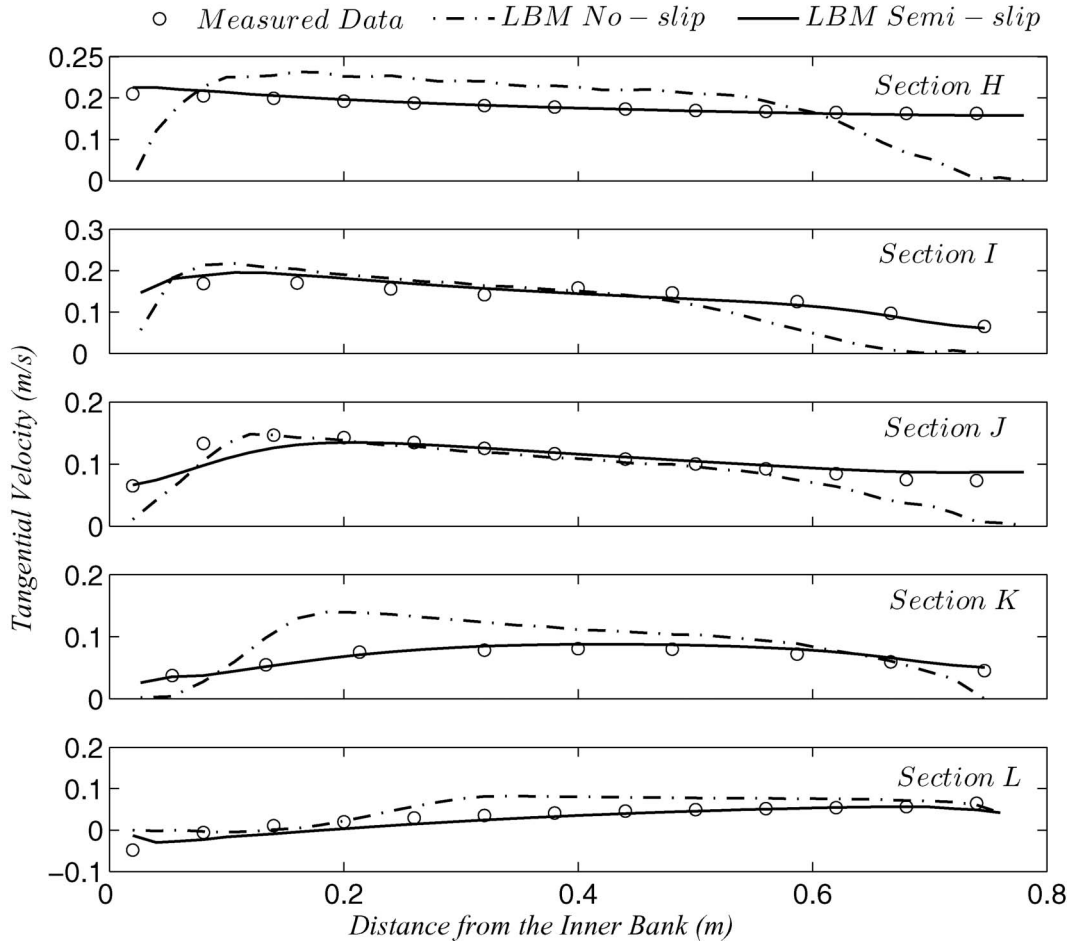

Figure 7. Transverse profiles of the depth-averaged tangential velocity across five sections of the 180° sharply curved channel.

discharge at the inlet. Additionally, the Chézy coefficient for bed roughness is 32 m^2/s (Chow 1959). Uniform 300×150 and 600×300 meshes with $\Delta x = \Delta y = 0.02$ m and $\Delta x = \Delta y = 0.01$ m are used. The time step Δt and the single relaxation time τ are 0.01 s and 0.5001, respectively. The semi-slip boundary condition is set at the channel bank with the roughness coefficient (C_w) of 0.03. Equation (10) is solved with the modified force term given in Equation (28).

A steady state has been reached after 6000 iterations. Figure 6 illustrates that the model based on different meshes gives similar results with the average fractional error for the coarse grid being 3.44%. As a second-order method with grid ratio being 2, the fractional error is equal to the grid convergence index (GCI) proposed by Roache (1994), i.e. GCI = 3.44% for the coarse grid. Comparisons between predicted and depth-averaged tangential velocities at five cross-sections are depicted in Figure 7, and show satisfactory agreement when using the semi-slip boundary condition. On the contrary, the error using the no-slip boundary condition is bigger, especially in the area near the bank. The detailed error for each section can be found in Table 1. When the flow enters the bend, the tangential velocity near the inner bank is larger than that near the outer bank. However, the peak of the tangential velocity of the cross-section moves to outer bank as the water flow proceeds around the bend. Finally, the area near the outer bank has the higher flow velocity in the tangential direction. The overall depth-averaged tangential velocity and the velocity vectors are plotted in Figure 8, and the flow pattern can be further depicted in the depth-averaged streamline contour shown in Figure 9.

Table 1. Error for Tangential Velocity of 180° Sharply Curved Flow (%).

Section	*H*	*I*	*J*	*K*	*L*
No-slip BC	8.1	7.5	7.3	7.8	7.7
Semi-slip BC	3.2	3.5	3.6	3.4	3.3

5.2. *Test 2: 60° meandering channel*

The experimental channel investigated by Tarekul Islam consisted of eighteen 60° circular bends (Tarekul Islam 2000, Tarekul Islam *et al.* 2000). The

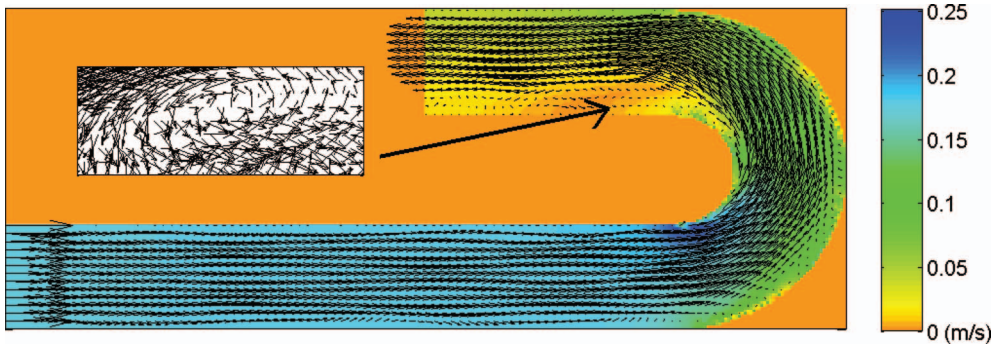

Figure 8. Plots of the depth-averaged tangential velocity (colour) and velocity vector (arrows) for 180° sharply curved channel.

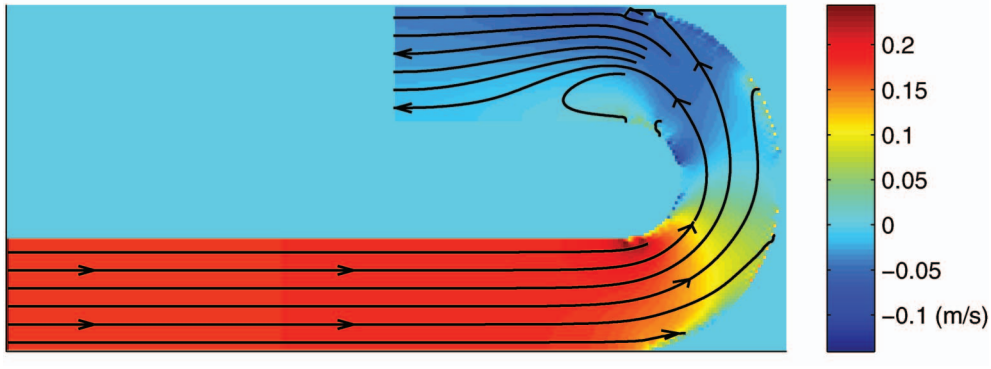

Figure 9. Plots of the depth-averaged longitudinal velocity (colour) and streamlines (arrows) for 180° sharply curved channel.

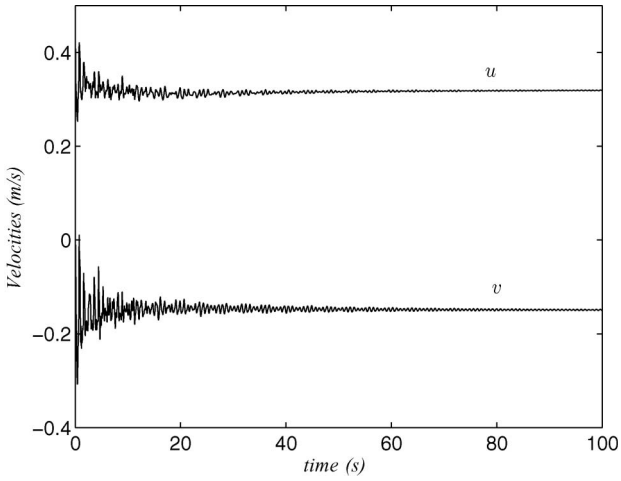

Figure 10. Velocity histories at test point $P_{(b)}$ in the centre of the channel.

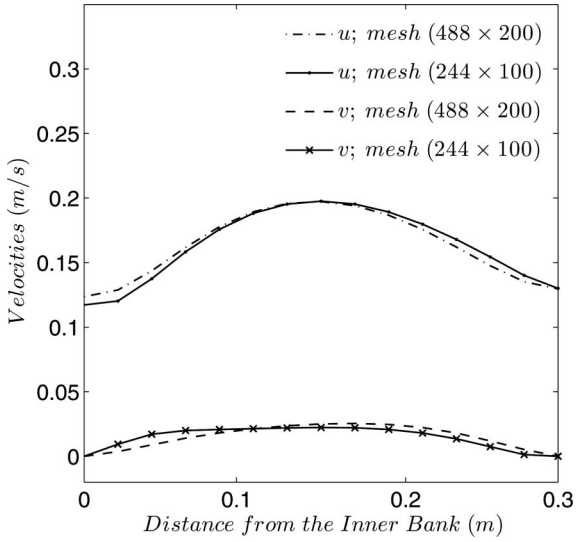

Figure 11. Comparison of the depth-averaged velocities across Section B (Figure 1) of the 60° meandering channel.

radius of curvature for channel centre line is 1.3 m. A 0.07 m straight reach is used to connect each bend. The cross-section of the meandering channel is a rectangle of 0.3 m width. The longitudinal gradient and the Manning's roughness are 0.001 and 0.008 $s/m^{1/3}$, respectively. The average water depth is 0.045 m for a constant discharge of 0.0051 m^3/s at the inlet. Since the Reynolds number is about 10,000 based on the experimental conditions, the single relaxation time, τ is set to 0.5001 and a slip boundary condition is used, i.e. $\xi = 1$. Time step and characteristic length are 0.01 s and 0.02 m.

A uniform 244 × 100 mesh is employed for calculations in four consecutive bends. After 10,000 computational iterations, the velocity histories of a particular point ($P_{(b)}$ in Figure 1(b)) in the channel certified that the result has converged to a steady state (see Figure 10). Compared with that using a 488 × 200 fine mesh, the grid convergence index (GCI) for the coarse gird is 3.68% in terms of the depth-averaged velocities (see Figure 11). The water depths and depth-averaged velocity profiles of three cross-sections (Section A, B and C) have been plotted in Figure 12 and Figure 13. It can be found that an excellent agreement has been achieved in terms of water depth, and the velocity differences between the numerical results and experimental data are small being only 6.1% for u and 2.6% for v on average (see Table 2). Because of the centripetal force, the water depth increases from the inner bank to the outer bank, so do the peaks of the longitudinal velocity. For all three cross-sections, the vertical velocities are nearly zero. In addition, the depth-averaged velocity vectors, based on the model with and without the second-order boundary treatment, have been plotted in Figure 14. It can be seen that the second-order boundary condition produces a more accurate result along the curved boundaries.

5.3. *Test 3: 90° meandering channel*

In this test, the experimental channel studied by Tamai *et al.* (1983) with ten 90° consecutive bends and a rectangular cross-section is selected. A straight reach closely follows each circular curve so that the central line of the channel is in the form of sine curve depicted in Figure 1(c). The radius of the curve is 0.6 m; the width of the channel is 0.3 m; the longitudinal slope is 0.001 and the roughness of the channel is estimated to be 0.013 $s/m^{1/3}$ for the Manning's coefficient. The average water depth and Froude number are 0.03 m and 0.42 respectively for a constant discharge of 0.02 m^3/s at the inlet. The single relaxation time, τ is set to 0.500393 and a no-slip boundary condition is used, i.e. $\xi = 0$. Time step and characteristic length are 0.005 s and 0.02 m, respectively. A uniform 300 × 120 mesh, which has the similar mesh density to that for the 60° meandering channel, has been generated for four consecutive bends. The downstream section was selected at the straight reach where the water depth is almost constant according to the experimental conditions. A steady state has been reached after 20,000 computational iterations.

The water depths and depth-averaged velocity profiles of three cross-sections (Sections *E, F* and *G* in Figure 1(c) are 15°, 30° and 45° from the longitudinal direction, respectively) have been plotted in Figure 15 and 16. As is indicated, a good agreement has been achieved for water depth with the maximum

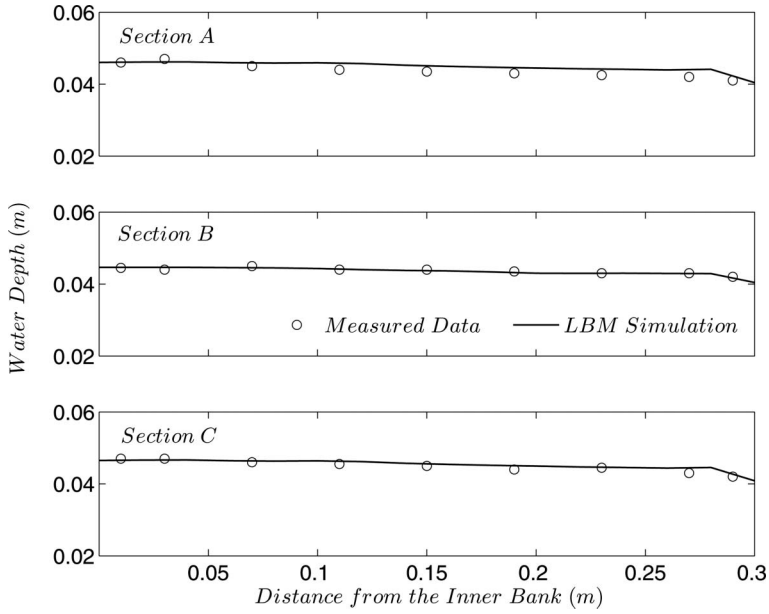

Figure 12. Water depth for meandering channel with 60° bends.

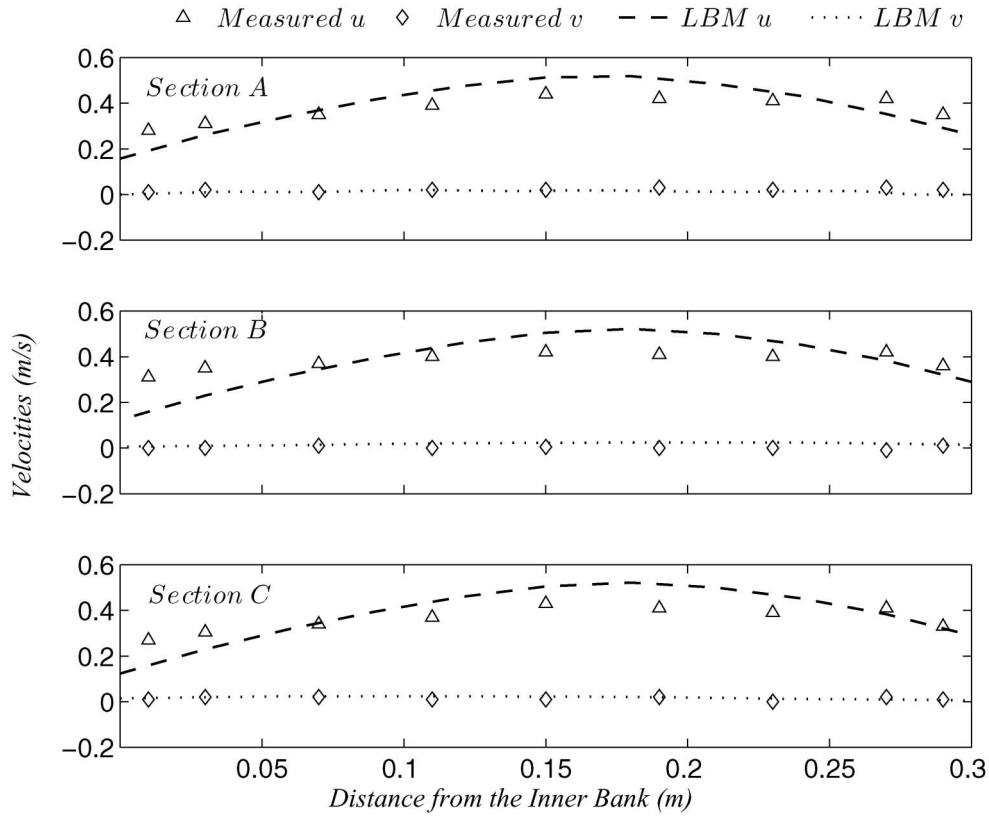

Figure 13. Transverse profiles of the depth-averaged velocity components across three sections of the meandering channel with 60° bend.

difference being only 3 mm. The water depth near outer bank is slightly larger than that near inner bank for all these three cross sections. The numerical results for longitudinal and lateral velocities are close to experimental data with the average error of 4.2% (see Table 2). Furthermore, the contours of the

Table 2. Error for Variables of 60° and 90° Meandering Channel Flows (%).

Section	*A*	*B*	*C*	*E*	*F*	*G*
Water depth *h*	2.2	1.5	1.6	3.3	3.0	3.1
Velocity *u*	6.2	6.3	5.9	5.4	5.7	5.3
Velocity *v*	2.6	2.5	2.8	2.9	2.9	2.8

velocities have been plotted in Figure 17, indicating that the peak of the longitudinal velocity occurs in the centre of each bend, whereas the absolute value of the lateral velocity reaches the maximum at the connection of two bends. The feature of the velocity field at a bend is further illustrated in Figure 18.

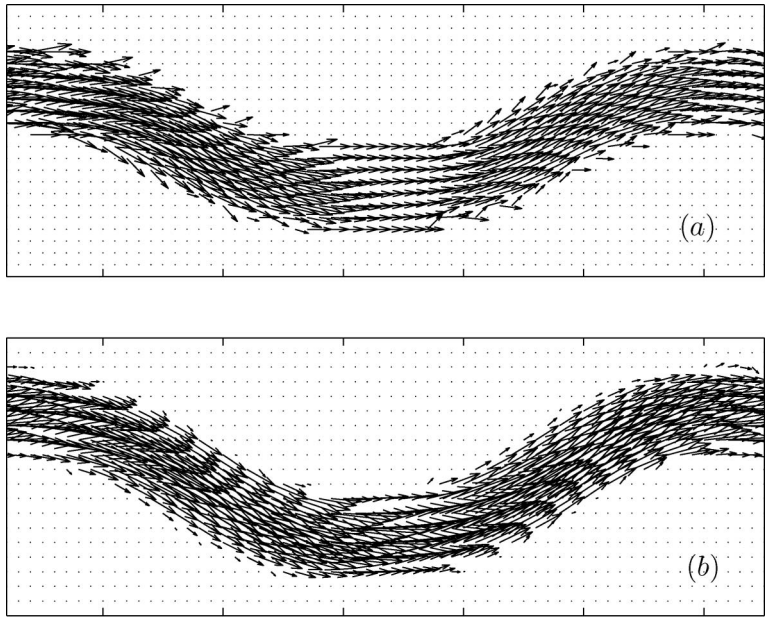

Figure 14. The depth-averaged velocity vector for the 60° meandering channel with (b) and without (a) the second-order boundary condition.

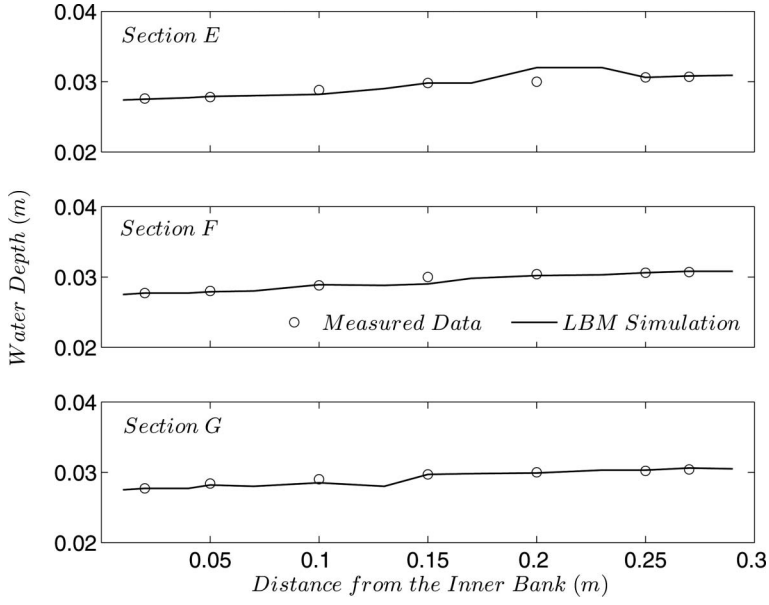

Figure 15. Water depth for meandering channel with 90° bends.

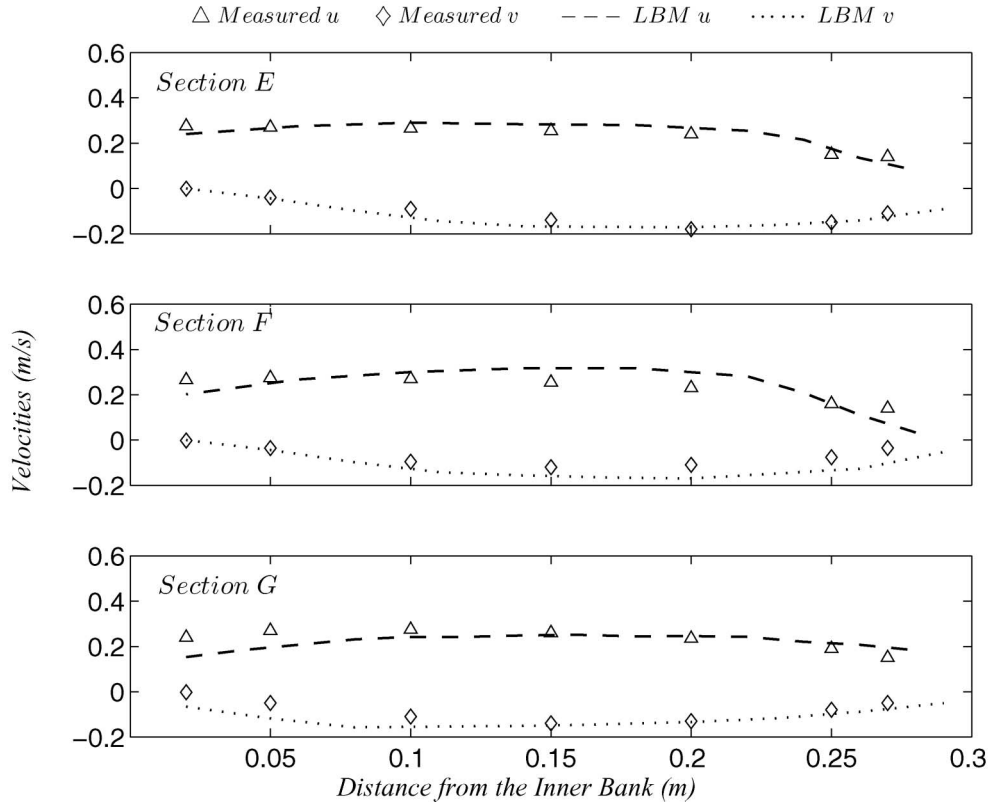

Figure 16. Transverse profiles of the depth-averaged velocity components across three sections of the meandering channel with 90° bends.

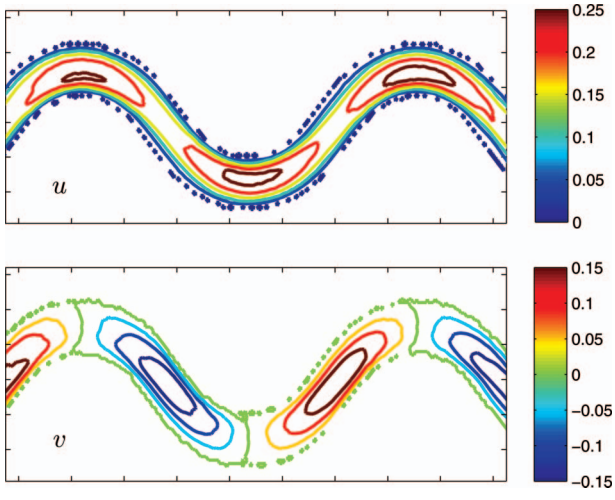

Figure 17. Contours of the depth-averaged velocities (m/s) for meandering channel with 90° bends.

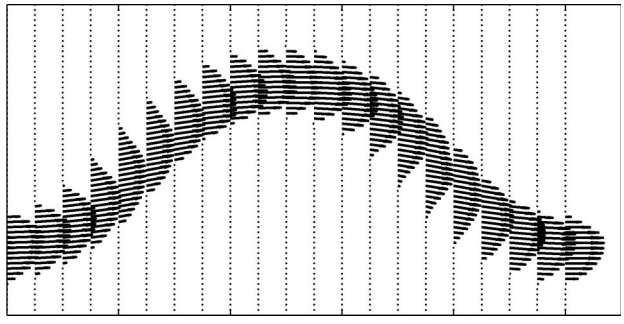

Figure 18. Plot of the depth-averaged velocity vector for a bend of the 90° meandering channel.

6. Conclusions

In this study, a two-dimensional lattice Boltzmann model with the second-order boundary conditions for meandering channel flow has been developed and validated, in which the large eddy simulation model is coupled with non-linear shallow water equations (LABSWE^{TM}) for turbulence modelling. Numerical simulations have been verified by three tests. Overall, it is found that the boundary treatment scheme for the curved boundary is capable of producing acceptable depth-averaged hydrodynamic characteristics of shallow water flow in curved and meandering channels over a wide range of bend angle. Specifically, the following features and conclusions can be summarised:

- As a two-dimensional depth-averaged model, the turbulence caused by the secondary flow

generated by curved channel along the vertical direction cannot be simulated effectively.

- The new scheme is tunable and can be applied to no-slip, semi-slip and slip boundary conditions.
- Good stability of the designed scheme for curved boundaries has been found in the numerical tests, even for flows with the high Reynolds number and strong turbulence.
- Numerical model predictions for water depth and velocity distributions agree well with experimental data, illustrating the effectiveness of the lattice Boltzmann model with the second-order boundary conditions.

References

Bhatnagar, P., Gross, E.P., and Krook, M.K., 1954. A model for collision processes in gases: I. Small amplitude processes in charged and neutral one-component system. *Physical Reviews*, 94, 511–525.

Bouzidi, M., Firdaouss, M., and Lallemand, P., 2001. Momentum transfer of a Boltzmann-lattice fluid with boundaries. *Physics of Fluids*, 13 (11), 3452–3459.

Callander, R.A., 1978. River meandering. *Annual Review of Fluid Mechanics*, 10, 129–158.

Chen, H., Chen, S., and Matthaeus, W.H., 1992. Recovery of the Navier-Stokes equations using a lattice-gas Boltzmann method. *Physical Review A*, 45, R5539–R5542.

Chen, S., Martinez, D., and Mei, R., 1996. On boundary conditions in lattice Boltzmann BGK model. *Physics of Fluids*, 8, 2527–2536.

Chen, S. and Doolen, G.D., 1998. Lattice Boltzmann method for fluid flows. *Annual Review of Fluids Mechanics*, 30, 329–364.

Chow, V.T., 1959. *Open channel hydraulics*. New York: McGraw-Hill.

Filippova, O. and Hänel, D., 1998. Grid refinement for lattice-BGK models. *Journal of Computational Physics*, 147, 219–228.

Frisch, U., Hasslacher, B., and Pomeau, Y., 1986. Lattice-gas automata for the Navier-Stokes equation. *Physical Review Letters*, 56 (14), 1505–1508.

Guo, Z., Zheng, C., and Shi, B., 2002. An extrapolation method for boundary conditions in lattice B method. *Physics of Fluids*, 14 (6), 2007–2010.

Maier, R.S., Bernard, R.S., and Grunau, D.W., 1996. Boundary conditions for the lattice Boltzmann method. *Physics of Fluids*, 8 (7), 1788–1801.

Martys, N.S. and Chen, H.D., 1996. Simulation of multicomponent fluids in complex three-dimensional geometries by the lattice Boltzmann method. *Physical Review E*, 53 (1), 743–750.

McNamara, G.R. and Zanetti, G., 1988. Use of the Boltzmann equation to simulate lattice-gas automata. *Physical Review Letters*, 61 (20), 2332–2335.

Mechlih, H. and Hay, D.R., 1994. Control of systems partially unknown: variable structure approach. *In*: *Proceedings of the American Control Conference*, Baltimore, MD, 1174–1175.

Mei, R., Luo, L.S., and Shyy, W., 1999. An accurate curved boundary treatment in the lattice Boltzmann method. *Journal of Computational Physics*, 155, 307–330.

Morvan, H., Pender, G.G., Wright, N., and Ervine, D.A., 2002. Three-dimensional hydrodynamics of meandering compound channels. *Journal of Hydraulic Engineering*, 128 (8), 674–682.

Qian, Y.H., D'Humieres, D., and Lallemand, P., 1992. Lattice BGK models for Navier-Stokes equation. *Europhysics Letters*, 17, 479–484.

Roache, P.J., 1994. Perspective: A method for uniform reporting of grid refinement studies. *Journal of Fluids Engineering*, 116, 405–413.

Rozovskii, I.L., 1961. *Flow of water in bends of open channels*. Jerusalem: (transl. by Israel Program for Scientific Translations).

Sterling, J.D., 1996. Stability analysis of lattice Boltzmann methods. *Journal of Computational Physics*, 123, 196–206.

Succi, S., 2001. *The lattice Boltzmann equation for fluid dynamics and beyond*. New York: Oxford University Press.

Szalmas, L., 2007. Slip on curved boundaries in the lattice Boltzmann model. *International Journal of Modern Physics C*, 18 (1), 15–24.

Tamai, N., Ikeuchi, K., Yamazaki, A., and Mohamed, A.A., 1983. Experimental analysis on the open channel flow in rectangular continuous bends. *Journal of Hydroscience and Hydraulic Engineering*, 2, 17–31.

Tarekul Islam, G.M., 2000. *Three-dimensional flow field in doubly meandering compound channel under steady and unsteady flow conditions*. Thesis (PhD). Department of Civil Engineering, University of Tokyo, Japan.

Tarekul Islam, G.M., Tamai, N., and Kobayashi, K., 2000. Hydraulic characteristics of a doubly meandering compound channel. *In*: *Proceeding of the 2000 Joint Conference on Water Research Engineering and Water Research Planning*. ASCE, Minneapolis.

Tutar, M. and Hold, A.E., 2001. Computational modelling of flow around a circular cylinder in sub-critical flow regime with various turbulence models. *International Journal of Numerical Methods in Fluids*, 35, 763–784.

Wolf-Gladrow, D.A., 2000. *Lattice-gas cellular automata and lattice Boltzmann models*. Verlag Berlin Heidelberg, Germany: Springer.

Yan, G.W., 2000. A lattice Boltzmann equation for waves. *Journal Computational Physics*, 161 (9), 61–69.

Yen, C.L. and Yen, B.C., 1971. Water surface configuration in channel bends. *Journal of Hydraulics Division American Society of Civil Engineers*, 97, 303–321.

Zarrati, A.R., Tamai, N., and Jin, Y.C., 2005. Mathematical modeling of meandering channels with a generalized depth averaged model. *Journal of Hydraulic Engineering, ASCE*, 131 (6), 467–475.

Zhang, X., Bengough, A.G., Crawford, J.W., and Young, I.M., 2002. A lattice BGK model for advection and anisotropic dispersion equation. *Advances in Water Resources*, 25, 1–8.

Zhou, J.G., 2002. A lattice Boltzmann model for the shallow water equations with turbulence modeling. *International Journal of Modern Physics C*, 13 (8), 1135–1150.

Zhou, J.G., 2004. *Lattice Boltzmann methods for shallow water flows*. Berlin, Germany: Springer.

Zhou, J.G. and Goodwill, I.M., 1997. A finite volume method for steady state 2D shallow water flows. *International Journal of Numerical Methods for Heat and Fluid Flow*, 7 (1), 4–23.

Ziegler, D.P., 1993. Boundary conditions for lattice Boltzmann simulations. *Journal of Statistical Physics*, 71 (5/6), 1171–1177.